Oxygen-induced refinement of α precipitates in an aged metastable β Ti-15-333 alloy

Kathleen Chou^a, Owen Neill^b, Emmanuelle A. Marquis^{a*}

^a Department of Materials Science and Engineering, University of Michigan, Ann Arbor, MI 48109 USA

Kathleen Chou Dow Building 2300 Hayward St. Ann Arbor, MI 48109 kachou@umich.edu

Phone: 248-925-7880

ORCID: 0000-0003-1974-4766

Owen Neill North University Building 1100 N University Ave Ann Arbor, MI 48103 okneill@umich.edu

Phone: 734-615-6657

ORCID: 0000-0001-6343-8817

Emmanuelle A. Marquis (Corresponding Author) Dow Building 2300 Hayward St. Ann Arbor, MI 48109

emarq@umich.edu Phone: 734-764-8717

ORCID: 0000-0002-6476-2835

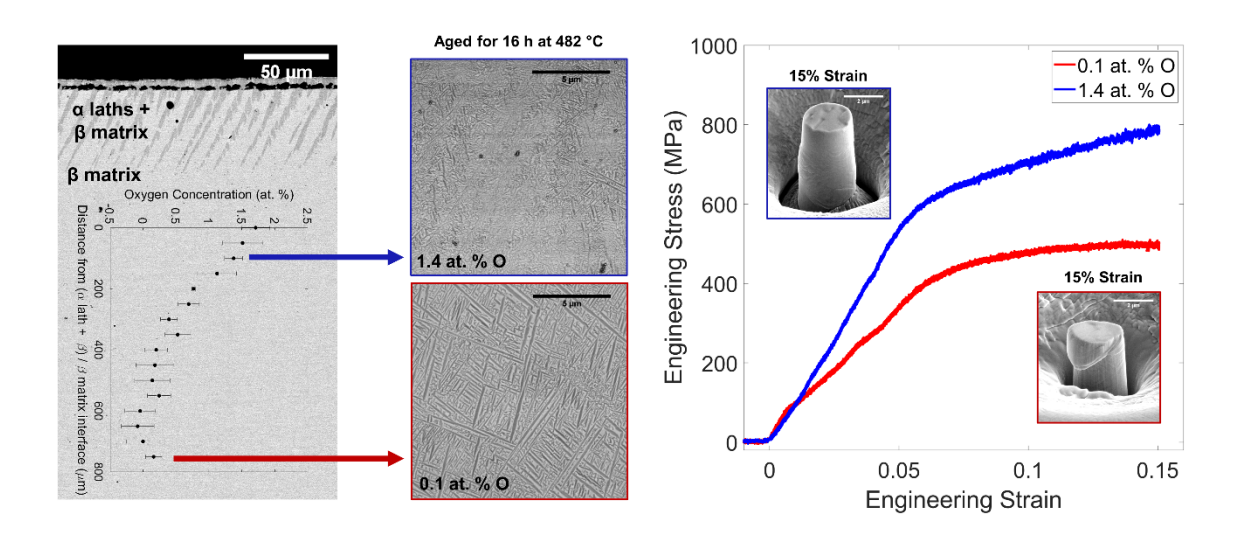
^b Department of Earth and Environmental Sciences, University of Michigan, Ann Arbor, MI 48103 USA

^{*}Corresponding Author

Oxygen-induced refinement of α precipitates in an aged metastable β Ti-15-333 alloy

Kathleen Chou^a, Owen Neill^b, Emmanuelle A. Marquis^{a*}

Graphical Abstract



Abstract

Increasing the strength of aged metastable β titanium alloys through refinement of intragranular α precipitates has been previously demonstrated using heterogeneous nucleation on structural and compositional non-uniformities. Here, we show that elevated oxygen levels (up to 1.7 at. %) can also induce α phase refinement during ageing of a β Ti-15-333 alloy, providing an additional pathway to obtain fine α laths. Moreover, oxygen-induced refinement combined with ω -assisted α nucleation resulted in significantly reduced α sizes of ~50 nm. The finer α precipitates obtained with higher oxygen concentrations resulted in increased compressive yield strengths during micropillar compression compared to specimens without oxygen. These findings highlight the use of high oxygen contents to improve α microstructural refinement and precipitation strengthening in β Ti alloys.

^a Department of Materials Science and Engineering, University of Michigan, Ann Arbor, MI 48109 USA

^b Department of Earth and Environmental Sciences, University of Michigan, Ann Arbor, MI 48103 USA

^{*}Corresponding Author

Keywords: Titanium alloys; Phase transformations; Precipitation; Compression test; Oxygen

Metastable β titanium alloys provide many opportunities for microstructural design and tailoring leading to a wide range of mechanical properties, enabling their use as structural materials for many applications [1-3]. Depending on chemistry and processing, these alloys exhibit desirable structural properties such as high specific-strength and ductility, hardenability, fatigue performance, and corrosion resistance [4]. The rich variety of attainable microstructures stems from the metastable β phase achieved through chemical alloying coupled with various thermomechanical treatments. During ageing, significant precipitation strengthening may occur from extensive intragranular α precipitation in the β matrix [1]. Many studies have focused on obtaining increasingly finer a precipitate sizes that yield very high strengths for applications such as aerospace components [1,2]. Specifically, the use of different heating rates, multi-step ageing treatments, ω-assisted α precipitation, and pseudospinodal mechanisms have been investigated to control α volume fraction, size, and number density [4–12]. With ω -assisted α nucleation mechanisms, previous investigations have focused on the influence of structural and compositional changes associated with ω phase formation to induce finer α precipitation [5,6,8]. It has also been hypothesized that oxygen-rich regions near ω embryos may assist the formation of α precipitates [13]. More generally, any structural and/or compositional heterogeneity can promote heterogeneous α nucleation, leading to higher nucleation rates and consequently increased refinement of α laths [1]. In addition, oxygen in concentrations of \sim 4 at. % was also shown to accelerate α precipitation yielding finer α precipitates in an aged Ti-20 at. % Nb alloy [14]. While it has been well reported that O causes solid solution hardening and ductility reduction in α-Ti alloys [15], the ductility of selected β Ti alloys is not jeopardized by high oxygen levels in the range of 2.5-3.0 at. % [16,17], enabling the use of oxygen in tailoring alloy microstructure and properties. In this study, we demonstrate the use of oxygen solid solutions to refine α precipitation during ageing in a commercial metastable β Ti alloy Ti-15-333, which is known to have excellent properties including cold deformability and high strength after ageing [18].

Commercial alloy Ti-15-333 (Ti-15V-3Cr-3Sn-3Al, wt. %) with nominally less than 0.1 wt. % O was provided by ATI. The β transus temperature for Ti-15-333 is reported as 750-770 °C

[19]. Specimens were sectioned using a slow speed diamond saw, encapsulated in quartz tubes with Ar gas, solution treated at 1000 °C for 24 h, and quenched by breaking the tube in water. A subset of solution treated samples were oxidized in a 1 standard cubic centimeter per minute (SCCM) O_2 /4 SCCM Ar (20% O_2) environment at 900 °C for 5 hours. The oxygen concentration profile in the β matrix after oxidation was measured on a polished cross-section using wavelength dispersive X-ray spectroscopy (WDS) using a Cameca SX100 electron microprobe as described in Ref. [14]. Measurements of the O K α , Ti K α , V K α , Cr K α , Al K α and Sn L α X-rays were made using a beam current of 40 nA and accelerating potential of 15 keV. Calibration standards were synthetic MgO (O K α), Ti metal (Ti K α), V metal (V K α), Cr metal (Cr K α), synthetic NiAl alloy (Al K α) and Sn metal (Sn L α); Additional WDS method details are located in **Supplementary Material**.

As-solution treated samples and oxidized samples were subsequently encapsulated in quartz tubes with Ar gas and aged using the following conditions: 250 °C for 64 h, and 482 °C for 16 h. Specimens were inserted into a preheated furnace such that the sample heating rate was > 5 °C/s. Aged specimens were cross-sectioned using a slow speed diamond saw, mounted in epoxy, ground using SiC papers, and polished using 0.03 µm colloidal silica suspension. Scanning electron microscope (SEM) imaging and focused ion beam (FIB) preparation of transmission electron microscopy (TEM) foils were performed using a Thermo Fisher Scientific Helios 650 Nanolab with a Ga⁺ ion FIB. TEM was performed using a Thermo Fisher Scientific Talos F200X G2 microscope operated at 200 kV.

Due to the compositionally graded nature of specimens created after oxidation, micropillar compression testing was used to assess the mechanical properties as a function of oxygen content. A specific grain close to the $(100)_{\beta}$ out of plane orientation was selected in each specimen using electron backscattered diffraction (EBSD) (**Supplementary Material**). Single crystal micropillars with a 2 μ m diameter were fabricated in the selected grains with a Thermo Fisher Scientific Helios 650 Nanolab using an automated script with coarse FIB annular milling at 30 kV, 9 nA and fine FIB milling at 30 kV, 0.79 nA. Milled micropillars had a diameter-to-height aspect ratio of approximately 1 to 2.5 to avoid a triaxial stress state for low aspect ratios and pillar buckling at high aspect ratios [20]. Micropillars were tested in compression in a Hysitron TI 950 Triboindenter with a flat punch indenter (60° cone angle, 10 μ m diameter flat end) in displacement-controlled

mode with a strain rate of $\sim 0.0005~\text{s}^{-1}$. Tests were manually stopped at a predetermined displacement corresponding to a specific strain level. Compressive engineering stress-strain curves were calculated from collected load versus displacement data [21]. After compression, deformed pillar morphologies were observed using SEM.

Solution-treated and quenched Ti-15-333 was exclusively made of the β phase with grain sizes greater than 500 µm. Previous work reported that as-quenched samples did not contain athermal ω phase [22]. However, electron diffraction from solution-treated and quenched Ti-15-333 (Figure 1) showed reciprocal lattice streaking and secondary intensity maxima at 1/3 and 2/3 {112}_β locations corresponding to ω diffraction spots [23]. A dark-field TEM image formed from the secondary intensity maxima (marked by the orange circle in Figure 1) confirmed the presence of nanoscale athermal ω precipitates. After oxidation at 900 °C, the oxide scale that formed on the sample's surface spalled easily during specimen handling and sectioning, leaving the base metal exposed and unprotected. Precipitation of a laths about 60 µm in length was observed in the subsurface metal below the oxide/metal interface (Figure 2a). Given oxygen's role as a significant α stabilizer in titanium alloys, the formation of α laths during oxidation is consistent with oxygen dissolution in the β Ti matrix during high temperature oxidation that subsequently stabilizes α and promotes its precipitation [24]. Below the α lath + β matrix region, the single-phase β matrix contained a concentration gradient of oxygen created through oxygen diffusion during the oxidation exposure. This concentration profile was measured in the β matrix using WDS starting from the α lath + β region near the sample's edges and moving towards the center of the crosssectioned specimens. The measurements (Figure 2b) illustrated that oxygen diffused to a depth of ~650 μ m during oxidation and reached a maximum interstitial oxygen level of ~1.7 at. % in the β matrix near the $\alpha + \beta$ region. This oxygen level is consistent with the maximum interstitial oxygen solubility in the β phase at 900 °C according to the O-Ti phase diagram [25]. WDS measurements showed no change for V, Cr, Sn, and Al levels in the single-phase β matrix (Supplementary Material).

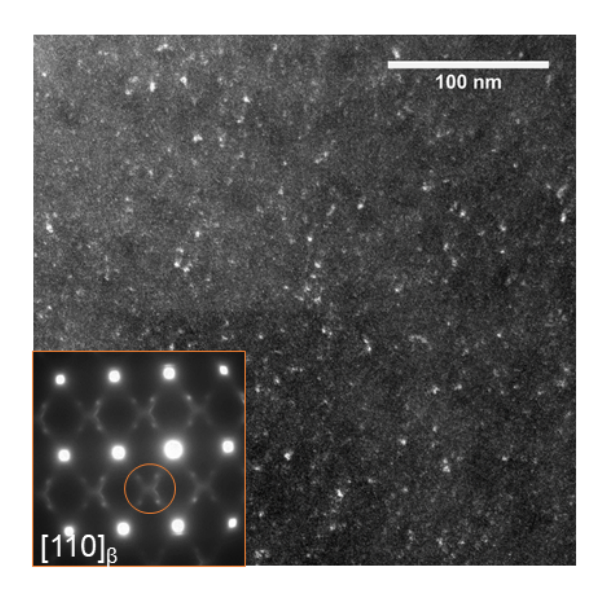


Figure 1. Dark-field TEM image and selected area electron diffraction (SAED) pattern of [110] $_{\beta}$ zone axis showing β and athermal ω diffraction spots for solution-treated and quenched Ti-15-333.

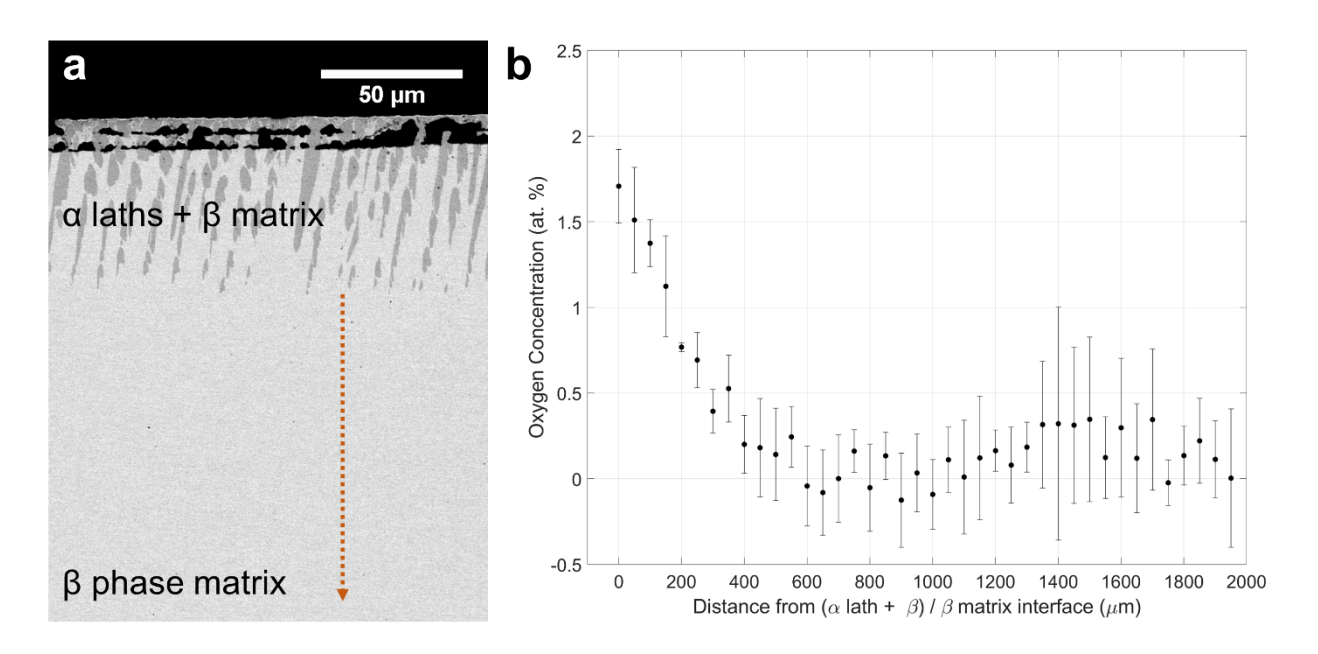


Figure 2. (a) Backscattered SEM (SEM-BSE) image of base metal after oxide spallation showing α lath formation after oxidation exposure at 900 °C for 5 h. Orange arrow indicates starting location and direction of WDS line traces. (b) Average of four WDS line traces measuring experimentally-induced oxygen concentration beginning from the (α lath + β) / β matrix interface and traversing across the cross-section of oxidized Ti-15-333.

As-solution treated specimens and oxidized specimens were subsequently aged directly at 482 °C for 16 h to promote α precipitation according to a commercial heat treatment [19]. The heat treatment (482 °C for 16 h) resides in the region where α precipitates are known to form directly from the β matrix [18,26]. 482 °C is also above the ω solvus according to Thermo-Calc calculations of metastable phase fractions (Supplementary Material). Fast heating to 482 °C also avoided β phase separation and isothermal ω evolution that are known to promote heterogeneous α nucleation [4,26,27]. Consequently, the athermal ω phase observed in solution treated specimens and oxidized specimens was expected to dissolve quickly upon rapid heating and ageing at 482 °C. Extensive intragranular α precipitation in the β matrix was observed regardless of oxygen content (Figure 3). In directly aged samples, α precipitates ranged from ~2-10 μ m in size. However, α precipitates became more refined with increasing oxygen content in the oxidized and aged Ti-15-333 sample. In regions containing little oxygen (0.1 at. %) near the center of this sample, α precipitates showed similar sizes as directly aged specimens aged with the same treatment. In regions with the highest oxygen content such as just below the α lath β matrix interface, corresponding to 1.7 at. % O, α laths were significantly smaller with submicron sizes. In the absence of β phase separation and ω precipitates that act as preferential nucleation sites, the observed α microstructural refinement is linked to the interstitial oxygen levels present in oxidized and aged Ti-15-333 rather than heterogeneous nucleation mechanisms. Interstitial oxygen in solid solution is known to significantly stabilize the α phase in Ti alloys [24]. This stabilization with elevated oxygen increases the nucleation driving force for a precipitation, leading to faster precipitation kinetics with a more refined lath size. Similar correlation was reported during isothermal oxidation of a β Ti Beta21S alloy with finer α laths forming in the β matrix near the surface where the oxygen content is the highest [28]. Changes in nucleation driving force have also been attributed to refined α precipitation in pseudospinodal transformation pathways [10,11], which are related to local composition fluctuations rather than intentional chemistry changes with oxygen. As a potent αstabilizing element, oxygen is known to partition to the α phase during ageing of β Ti alloys [29], so very little oxygen is expected in the β matrix after α formation during ageing.

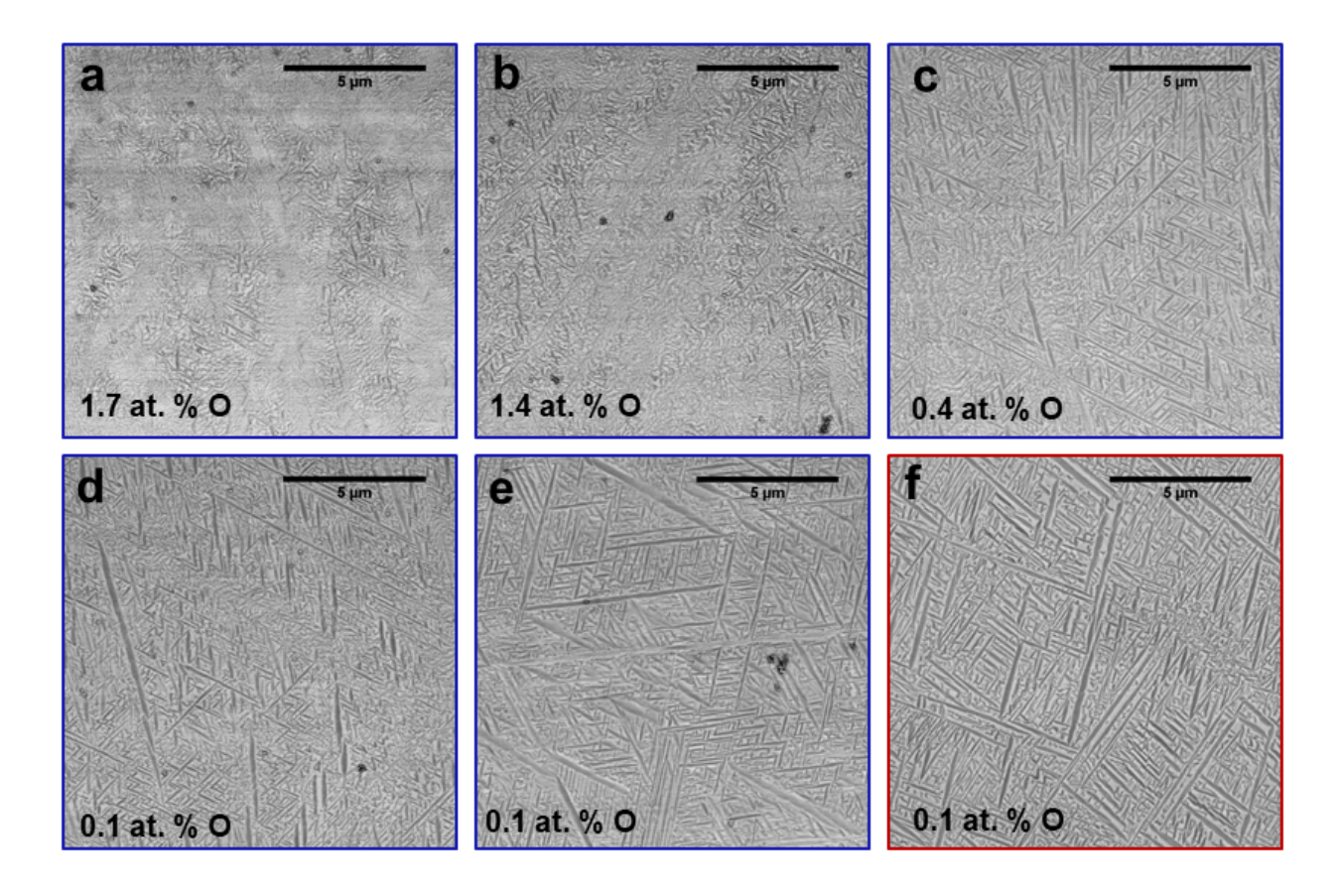


Figure 3. SEM-BSE images of oxidized and aged Ti-15-333 aged for 16 h at 482 °C located (a) at the α lath/β matrix interface, (b) 100 μm, (c) 300 μm, (d) 500 μm from this interface, and (e) in the center of the sample. Oxygen concentrations for (a-e) correspond to 1.7, 1.4, 0.4, 0.1, and 0.1 at. % O, respectively, from WDS measurements. (f) SEM-BSE image of directly aged Ti-15-333 with 0.1 at. % O aged for 16 h at 482 °C.

After ageing directly at 482 °C, directly aged and oxidized and aged Ti-15-333 were tested using micropillar compression to estimate local mechanical behavior (**Figure 4a-b**). For oxidized and aged specimens, micropillars were produced at a distance of 100 μ m away from the α lath / β matrix interface corresponding to 1.4 at. % O. After compression to 15% strain, deformed pillars for directly aged and oxidized and aged Ti-15-333 (**Figure 4c-d**) both showed slip traces located near α - β interfaces. Previously reported micropillar compression results for dual phase α - β Ti alloys also showed that α - β microstructures typically slip along the interface between these phases if oriented favorably relative to the deformation direction [30–32]. However, significant morphology differences were observed for compressed pillars depending on initial microstructure

and oxygen content. Directly aged micropillars formed macroscopic slip bands spanning the entire pillar diameter due to the larger α lath sizes present without oxygen (**Figure 4c**). In contrast, the refined α precipitates in compressed pillars for oxidized and aged Ti-15-333 with 1.4 at. % O resulted in numerous shorter slip traces that formed in multiple locations along the pillar's length leading to slight bulging (**Figure 4d**), indicating more distributed deformation compared to directly aged pillars.

Compressive engineering stress-strain curves revealed that the refined α sizes obtained with higher oxygen content increased the compressive yield strength, from an average value of ~390 MPa for pillars without oxygen to 580 MPa in the presence of 1.4 at. % O. Figure 4e shows curves closest to the average yield strength out of four tested micropillars for each condition. We note the observed differences in ductility for the stress-strain curves, but these differences are not informative due to limitations of micropillar compression testing methodology [33], so these results are only used to compare trends for compressive yield strength. Scatter in the stiffness and yield point values was observed in the stress-strain curves at both oxygen levels, which was attributed to intrinsic size effects stemming from the tested micropillar sizes and volumes. Indeed, intrinsic size effects can dominate when specimen dimensions are on the order of microstructural features and the specimen's volume contains a lower number density of dispersed obstacles, leading to an observed size effect on measured yield strengths [34]. Nonetheless, the increased α refinement results in more α - β interfaces that act as dislocation barriers resulting in increased strength [2,9,24]. This trend in yield strength values is consistent with prior mechanical testing of β Ti alloys where higher densities and increased refinement of α precipitates resulted in increased bulk tensile strength [1,4,9] and micropillar compression strength [31,32]. Consistently, indentation studies of oxygen-enriched sublayers formed during oxidation of other commercial metastable β Ti alloys correlated to hardness increases with refined α precipitation [28,35].

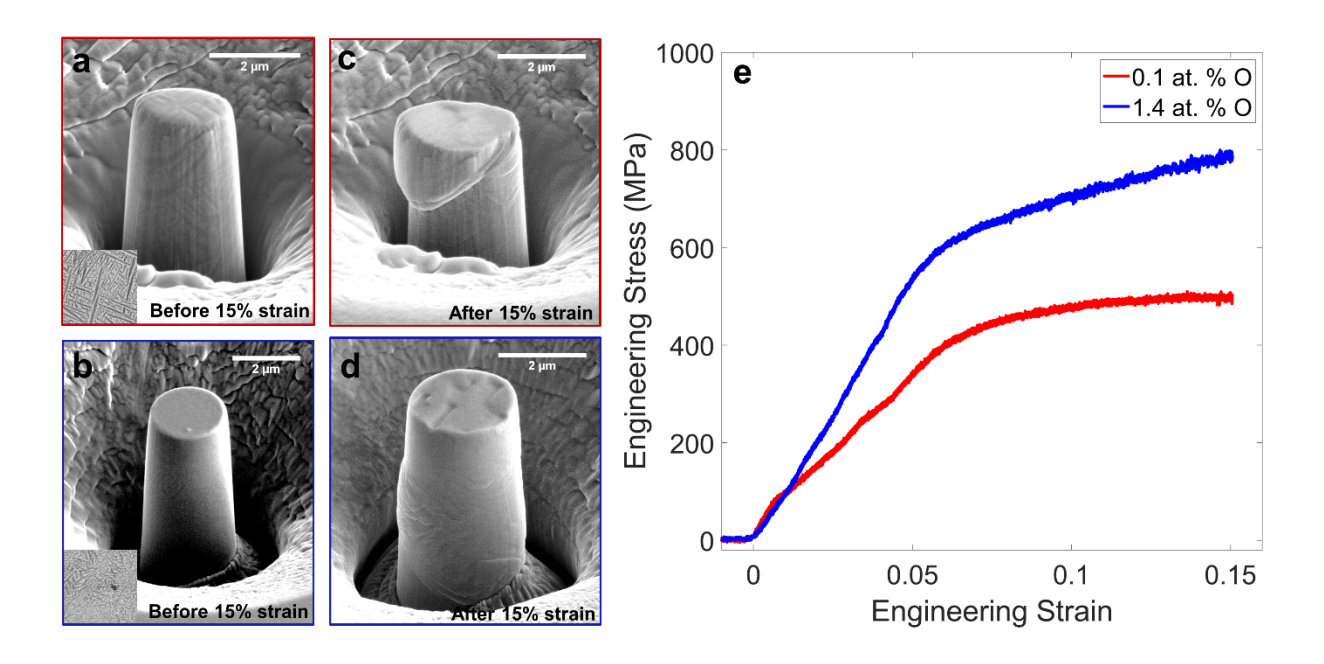


Figure 4. SEM-BSE images of 2 μm diameter micropillars compressed to 15% engineering strain for (a, c) directly aged Ti-15-333 with 0.1 at. % O and (b, d) oxidized and aged Ti-15-333 with 1.4 at. % O aged for 16 h at 482 °C before (a-b) and after (c-d) compression. Insets for (a-b) show SEM-BSE images of initial microstructure for each pillar. (e) Engineering stress-strain curves for compressed micropillars on directly aged Ti-15-333 with 0.1 at. % O and oxidized and aged Ti-15-333 with 1.4 at. % O aged for 16 h at 482 °C.

Finally, double ageing was conducted to understand the combined effects of ω -assisted α nucleation and oxygen-induced α refinement. Ageing of directly aged Ti-15-333 at 250 °C for 64 hours promoted chemical partitioning and growth of isothermal ω precipitates around ~5-10 nm in size (**Figure 5a-b**). With oxygen's reported stabilization of the ω phase [14], isothermal ω was also expected to be present in oxidized and aged Ti-15-333 aged at 250 °C for 64 h. Following the low temperature treatment, directly aged and oxidized and aged specimens were aged at 482 °C for 16 h. Irrespective of oxygen content, fine α precipitates were observed after the final 482 °C ageing step (**Figure 5c-d**). The α laths were approximately 300 nm in size for the directly aged specimens, while those in the oxidized and aged specimens with 1.4 at. % O were even smaller at ~50 nm. The observed refined α sizes in the directly aged and oxidized and aged samples are attributed to ω -assisted α nucleation, in which the structural and compositional non-uniformities stemming from isothermal ω formation act as preferred sites for heterogeneous intragranular α nucleation [4–6,8]. Notably, oxygen-containing Ti-15-333 showed further α microstructural

refinement compared to oxygen-free specimens even though ω -assisted nucleation was active in both conditions, which suggests that oxygen-induced refinement can be used in tandem with other α refinement methods.

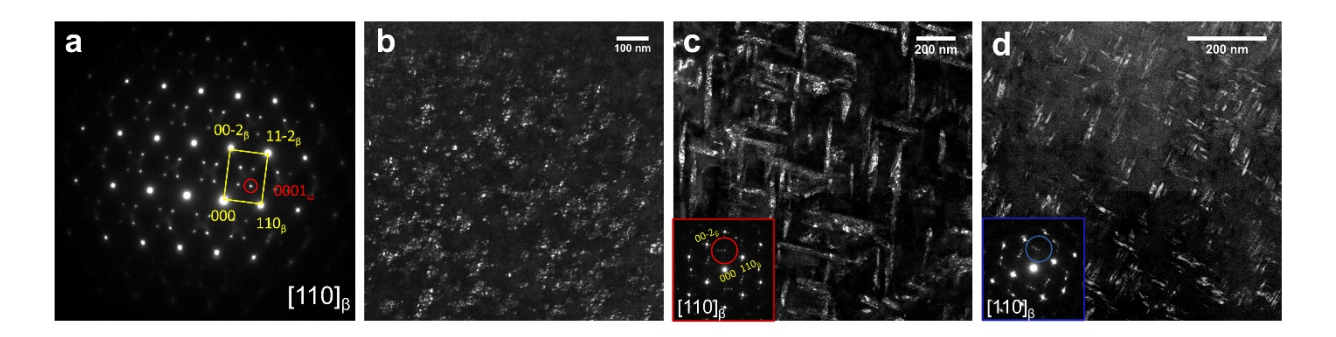


Figure 5. (a) TEM SAED pattern for the $[110]_{\beta}$ zone axis showing β and ω diffraction spots for directly aged Ti-15-333 with 0.1 at. % O aged for 64 h at 250 °C. (b) Dark-field TEM image formed using the selected ω diffraction spot shown in the red circle of (a). (c) TEM SAED pattern for the $[110]_{\beta}$ zone axis and dark-field TEM image formed using the selected diffraction spots shown in the red circle revealing fine α laths for directly aged Ti-15-333 with 0.1 at. % O aged for 64 h at 250 °C, then for 16 h at 482 °C. (d) TEM SAED pattern for the $[110]_{\beta}$ zone axis and dark-field TEM image formed using the selected diffraction spots shown in the blue circle revealing more refined α laths for oxidized and aged Ti-15-333 with 1.4 at. % O aged for 64 h at 250 °C, then for 16 h at 482 °C.

This study illustrates the ability of interstitial oxygen in metastable β Ti alloys to create fine α lath microstructures with increased compressive yield strength. Bulk tensile testing of microstructures with oxygen-induced α refinement would be necessary to confirm increases in strength without ductility reductions. However, oxygen's partitioning behavior from the β phase matrix to α precipitates during ageing [29] likely results in minimal oxygen in solid solution for the β phase matrix after ageing at 482 °C. Consequently, intentional additions of oxygen to metastable β Ti alloys may act as another avenue for obtaining α phase refinement during ageing and improved precipitation strengthening. Furthermore, this oxygen-induced refinement mechanism may be used in combination with existing α refinement strategies during ageing such as ω -assisted nucleation to obtain significantly reduced α sizes, as demonstrated with multi-step

ageing treatments (**Figure 5d**). Extensive studies on oxygen containing β Ti alloys have demonstrated strength increases without ductility reductions for annealed conditions [16,17] as well as suppression of shape memory behavior leading to increased superelasticity [36–38]. The present findings illustrate beneficial effects of oxygen specifically for aged metastable β Ti alloys resulting in microstructural refinement and increased strength. These results provide additional evidence that may contradict the conventional wisdom that oxygen levels in Ti alloys need to always be kept very low.

In summary, elevated oxygen levels obtained through an oxidation exposure increased the nucleation driving force for α precipitation during ageing, leading to microstructures with refined α precipitates obtained with and without activation of ω -assisted α nucleation. The use of oxygen to refine α lath sizes illustrates an additional pathway to obtain α microstructural refinement in aged β Ti alloys. Furthermore, these microstructures showed increased compressive strength during micropillar compression compared to those without oxygen due to a higher number of α - β interfaces that act as dislocation barriers, which suggests that the oxygen-induced α refinement may result in improved mechanical properties.

Acknowledgements

This work was supported by funding from the National Science Foundation (NSF) through grant NSF CMMI-1729166 and the Graduate Research Fellowship Program under grant No. DGE 1256260. The authors would also like to thank Dr. John Foltz at ATI for providing the Ti-15-333 alloy material and the Michigan Center for Materials Characterization and the Electron Microbeam Analysis Laboratory at the University of Michigan for use of electron microscopy and electron microprobe facilities.

References

- [1] R. Kolli, A. Devaraj, Metals (Basel). 8 (2018) 506.
- [2] J.D. Cotton, R.D. Briggs, R.R. Boyer, S. Tamirisakandala, P. Russo, N. Shchetnikov, J.C. Fanning, Jom 67 (2015) 1281–1303.
- [3] M. Niinomi, M. Nakai, J. Hieda, Acta Biomater 8 (2012) 3888–3903.

- [4] O.M. Ivasishin, P.E. Markovsky, Y.V. Matviychuk, S.L. Semiatin, C.H. Ward, S. Fox, J. Alloys Compd. 457 (2008).
- [5] F. Prima, P. Vermaut, G. Texier, D. Ansel, T. Gloriant, Scr. Mater. 54 (2006).
- [6] T. Li, D. Kent, G. Sha, L.T. Stephenson, A. V Ceguerra, S.P. Ringer, M.S. Dargusch, J.M. Cairney, Acta Mater. 106 (2016) 353–366.
- [7] A. Devaraj, S. Nag, R. Banerjee, Scr. Mater. 69 (2013).
- [8] Y. Zheng, R.E.A. Williams, D. Wang, R. Shi, S. Nag, P. Kami, J.M. Sosa, R. Banerjee, Y. Wang, H.L. Fraser, Acta Mater. 103 (2016) 850–858.
- [9] S.A. Mantri, D. Choudhuri, T. Alam, G.B. Viswanathan, J.M. Sosa, H.L. Fraser, R. Banerjee, Scr. Mater. 154 (2018) 139–144.
- [10] S. Nag, Y. Zheng, R.E.A. Williams, A. Devaraj, A. Boyne, Y. Wang, P.C. Collins, G.B. Viswanathan, J.S. Tiley, B.C. Muddle, R. Banerjee, H.L. Fraser, Acta Mater. 60 (2012).
- [11] A. Boyne, D. Wang, R.P. Shi, Y. Zheng, A. Behera, S. Nag, J.S. Tiley, H.L. Fraser, R. Banerjee, Y. Wang, Acta Mater. 64 (2014).
- [12] C.A.F. Salvador, V.C. Opini, M.G. Mello, R. Caram, Mater. Sci. Eng. A 743 (2019).
- [13] T. Li, D. Kent, G. Sha, H. Liu, S.G. Fries, A. V Ceguerra, M.S. Dargusch, J.M. Cairney, Scr. Mater. 155 (2018) 149–154.
- [14] K. Chou, E.A. Marquis, Acta Mater. 181 (2019) 367–376.
- [15] H. Conrad, Prog. Mater. Sci. 26 (1981) 123–403.
- [16] V. Jablokov, N. Murray, H. Rack, H. Freese, J. ASTM Int. 2 (2005) 12776.
- [17] T. Saito, T. Furuta, J.H. Hwang, S. Kuramoto, K. Nishino, N. Suzuki, R. Chen, A. Yamada, K. Ito, Y. Seno, T. Nonaka, H. Ikehata, N. Nagasako, C. Iwamoto, Y. Ikuhara, T. Sakuma, Science (80-.). 300 (2003) 464–467.
- [18] T. Furuhara, T. Maki, T. Makino, J. Mater. Process. Technol. 117 (2001).
- [19] Https://Www.Timet.Com/Assets/Local/Documents/Datasheets/Metastablebetaalloys/15-3.Pdf (n.d.).
- [20] H. Zhang, B.E. Schuster, Q. Wei, K.T. Ramesh, Scr. Mater. 54 (2006) 181–186.
- [21] W. Chen, J. Zhang, S. Cao, Y. Pan, M. Huang, Q. Hu, Q. Sun, L. Xiao, J. Sun, Acta Mater. 117 (2016) 68–80.
- [22] X. Wu, J. del Prado, Q. Li, A. Huang, D. Hu, M.H. Loretto, Acta Mater. 54 (2006).
- [23] A. Devaraj, S. Nag, R. Srinivasan, R.E.A. Williams, S. Banerjee, R. Banerjee, H.L. Fraser, Acta Mater. 60 (2012) 596–609.
- [24] D. Banerjee, J.C. Williams, Acta Mater. 61 (2013) 844–879.
- [25] J.L. Murray, H.A. Wriedt, J. Phase Equilibria 8 (1987) 148–165.

- [26] O.M. Ivasishin, P.E. Markovsky, Y. V. Matviychuk, S.L. Semiatin, Metall. Mater. Trans. A 34 (2003) 147–158.
- [27] O.M. Ivasishin, P.E. Markovsky, S.L. Semiatin, C.H. Ward, Mater. Sci. Eng. A 405 (2005).
- [28] A. Behera, S. Nag, K. Mahdak, H. Mohseni, J. Tiley, R. Banerjee, J. Mater. Sci. 48 (2013).
- [29] M. Niinomi, M. Nakai, M. Hendrickson, P. Nandwana, T. Alam, D. Choudhuri, R. Banerjee, Scr. Mater. 123 (2016) 144–148.
- [30] T.-S. Jun, G. Sernicola, F.P.E. Dunne, T.B. Britton, Mater. Sci. Eng. A 649 (2016).
- [31] W. Kou, Q. Sun, L. Xiao, J. Sun, J. Alloys Compd. 820 (2020) 153421.
- [32] W. Kou, Q. Sun, L. Xiao, J. Sun, Sci. Rep. 9 (2019).
- [33] M.D. Uchic, P.A. Shade, D.M. Dimiduk, Annu. Rev. Mater. Res. 39 (2009) 361–386.
- [34] J.P. Wharry, K.H. Yano, P. V Patki, Scr. Mater. 162 (2019) 63–67.
- [35] P. Samimi, D.A. Brice, I. Ghamarian, Y. Liu, P.C. Collins, Oxid. Met. 85 (2016).
- [36] L.S. Wei, H.Y. Kim, T. Koyano, S. Miyazaki, Scr. Mater. 123 (2016) 55–58.
- [37] P. Castany, A. Ramarolahy, F. Prima, P. Laheurte, C. Curfs, T. Gloriant, Acta Mater. 88 (2015) 102–111.
- [38] B. Yuan, B. Yang, Y. Gao, M. Lai, X.H. Chen, M. Zhu, Mater. Des. 92 (2016).